The first non-coherent precipitate, θ', was detected after 303 hours at 130 °C plus 24 hours at 200 °C. On the basis of the (004) θ' reflection measured in this work, the c parameter of θ' is $5{\cdot}84 \pm 0{\cdot}01$ Å.

During the growth of $GP2$ a diffuse maximum existed at an angle which corresponded to plane spacings of 1·27 Å (B in Fig. 1). This maximum became very weak after the formation of θ' and was completely absent after the equilibrium $CuAl_2$ was formed. Diffuse maxima have been reported in θ' before (Guinier, 1942), and the present authors propose the following explanation based on the results of this work. Based on the 1·27 Å spacing, the diffuse maximum observed during $GP2$ growth can be explained by a coherent 'matching' of 6 $GP2$ planes and 5 matrix planes (*i.e.* a 6th order reflection from a pseudo-lattice of 10·1 Å spacing). The diffuse maximum during θ' growth is explained by a similar coincidence of 8 θ' planes with 6 matrix planes (8th order reflection). The above configurations were chosen since they represent the lowest possible coherency strains between the existing GP structure and the matrix.

The sequence of transformation is seen to be gradual and tends toward a state of lower strain energy. As shown in Table 2, the copper content during the formation of $GP1$ gradually decreases to the approximate equilibrium composition as the diameter of the zone increases. At this stage an ordering of the Cu atoms takes place along with an increase in size of the zone and produces enough lattice misfit to form a non-coherent configuration.

The authors wish to acknowledge the Air Force Institute of Technology and the Advanced Research Projects Agency, Department of Defense, Contract SD-102, for their support of this investigation.

References

COCHRAN, W. (1956). *Acta Cryst.* **9**, 259.
DOI, K. (1960). *Acta Cryst.* **13**, 45.
GEROLD, V. (1958). *Acta Cryst.* **11**, 230.
GUINIER, A. (1942). *J. Phys. Radium*, **3**, 124.
SILCOCK, J. (1953). *J. Inst. Metals*, **82**, 239.
THOMAS, A. D. (1961). Ph. D. Thesis, Purdue University, Lafayette, Indiana.
TOMAN, K. (1957). *Acta Cryst.* **10**, 187

Acta Cryst. (1965). **18**, 681

A Three-Dimensional Analysis of Instrumental Broadening in X-Ray Measurements

BY GERALD L. LIEDL* AND PEKKA RAUTALA†

Purdue University, Lafayette, Indiana, U.S.A.

(*Received* 22 *June* 1964)

The effects of the source distribution, divergence slits, Soller slits, source width at the specimen, and absorption were interpreted as a three-dimensional measuring function in reciprocal space. The analysis of these instrumental effects was calculated for a particular set of instrumental coordinates chosen to minimize the number of instrumental effects along the paths of measurements.

The effect of the measuring functions for monochromatic radiation along the coordinates chosen was shown for cleaved single crystals of calcite and zinc. The measurements verify the proposed analysis and illustrate the three-dimensional character of the measurements.

Introduction

The experimental conditions of any diffraction experiment require finite source and receiving openings which result in divergent beams. Consequently, the conditions for diffraction may be fulfilled over a range of angles defined in part by these openings, *i.e.* by the instrument. The region in reciprocal space which does give rise to scattering is restricted by both the instrument and the specimen. The instrument defines the maximum possible region while the specimen may restrict the active region to some smaller portion of the maximum region.

The region defined by the instrument is three-dimensional, and for any real specimen, the active region defined by the specimen is also three-dimensional. Therefore, any diffraction measurement is inherently a three-dimensional measurement of the scattered intensity over a finite region, *i.e.* a power. The authors feel strongly that this three-dimensional nature of the measurements must be considered in the interpretation of the diffraction effects.

The elimination of instrumental effects in diffraction studies has been confined mainly to a one-dimensional analysis. The early work of Spencer (1931, 1939,

* Assistant Professor of Metallurgical Engineering, Purdue University, Lafayette, Indiana, U.S.A.

† Formerly Professor at Purdue University, Lafayette, Indiana. Present address: Tapiola, Finland.

1949) and Jones (1938) was developed and extended by Alexander (1948, 1950, 1954) for the one-dimensional case. The work of Jones (1938) on the use and evaluation of convolutions was clarified by Stokes (1948). More recently, Alexander & Smith (1962) made an extensive study of the one-dimensional instrumental effects in a three-circle goniometer. Outside of the one-dimensional studies, a three-dimensional study was made by Rautala & Hyvärinen (1955). The present study, based on the work of Rautala & Hyvärinen (1955), is concerned with the systematic elimination of the instrumental effects along three independent coordinates. The coordinates for this study were chosen to minimize the number of instrumental variables which would effect the measurements along each coordinate. Unfortunately, the coordinate systems which simplify an instrumental analysis are not, in general, the same coordinate systems which simplify the interpretation of the diffraction effects. However, the simplification is useful to illustrate the instrumental effects.

Theory

First, let us consider the geometrical interpretation of diffraction in terms of the equation

$$\mathbf{b}=(\mathbf{S}-\mathbf{S}_0)/\lambda$$

where $\mathbf{S}$ and $\mathbf{S}_0$ are vectors representing the directions of the diffracted and incident beams respectively, λ the wavelength, and $\mathbf{b}$ a vector in reciprocal space. The effect of the instrumental response may be interpreted as imparting a weighted variation in the directions of $\mathbf{S}$ and $\mathbf{S}_0$. Therefore, the instrument will be capable of measuring over a region determined by this variation as

$$\mathbf{M}(\gamma_1, \gamma_2, \gamma_3)=\mathbf{S}(\gamma_1, \gamma_2, \gamma_3)-\mathbf{S}_0(\gamma_1, \gamma_2, \gamma_3)\,. \quad (1)$$

The three angular coordinates in equation (1) are shown in Fig. 1. These coordinates form a basis to define $\mathbf{S}$ and $\mathbf{S}_0$, and consequently, $\mathbf{M}$ may be defined on the same basis. These three angles for a horizontal goniometer correspond to a rotation of the primary beam about the vertical axis, γ_1, a rotation of the detector about the vertical axis, γ_2, and a rotation of the specimen about a normal to the specimen surface, γ_3. Fig. 2 shows the γ_1, γ_2 coordinates in reciprocal space for a constant γ_3. We shall follow the practice that γ' is a fixed value of γ, and $\bar{\gamma}$ is another variable coincident with γ.

Let us now consider the effect of the divergence of $\mathbf{S}_0$ on the classical Fraunhofer intensity. Since the primary radiation is divergent, the divergence and the intensity of the primary beam may be described by a function. For the case of a vertical line source with a divergence slit and Soller slits, the function may be given as $f(\gamma_1)\,.\,L_p(\gamma_p)$. The function $f(\gamma_1)$ describes the variation in the direction of the divergence slit, and the function $L_p(\gamma_p)$ describes the variation in the direction of the Soller slits where γ_p is an angle in the direction of limiting divergence of the primary Soller slits.

In addition, the intensity is affected by absorption and the finite area of the irradiated region. Consequently, any part or all of these directions may give rise to the scattered intensity as

$$I(\gamma_1', \gamma_2', \gamma_3')=\iiint I(\gamma_1, \gamma_2, \gamma_3)\,f(\gamma_1'-\gamma_1)\,L_p(\gamma_p'-\gamma_p)\,A(\gamma_1'-\gamma_1, \bar{\gamma}_2-\gamma_2')\,d\gamma_1 d\gamma_p d\bar{\gamma}_2 \quad (2)$$

where $A(\gamma_1, \gamma_2)$ is a function describing the broadening due to absorption and the finite size of the irradiated region, and $I(\gamma_1, \gamma_2, \gamma_3)$ is the classical Fraunhofer intensity.

Since the receiving divergence and Soller slits must have a finite width, the total power measured is

$$P(\gamma_1', \gamma_2', \gamma_3') = \iint I(\gamma_1', \gamma_2, \gamma_3)\,S\left(\frac{\gamma_2'-\gamma_2}{a_r}\right) L_r(\gamma_r'-\gamma_r)\,d\gamma_2 d\gamma_r \quad (3)$$

where the variation in response of the detector is assumed to be negligible, $L_r(\gamma_r'-\gamma_r)$ describes the effect of the secondary Soller slits, a_r is the angular width of divergence slit, and

$$S\left(\frac{\gamma}{c}\right)=\begin{cases}1, & |\gamma|<c\\ \frac{1}{2}, & |\gamma|=c\\ 0, & |\gamma|>c\end{cases}$$

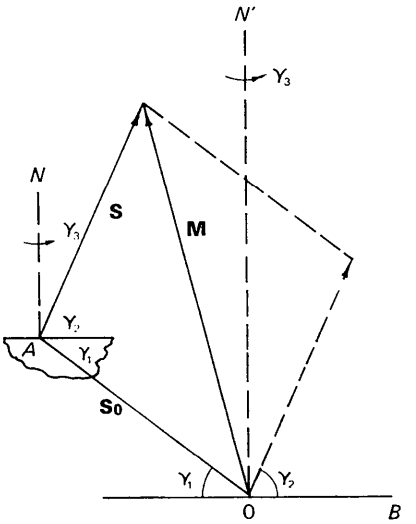

Fig. 1. The instrumental rotations.

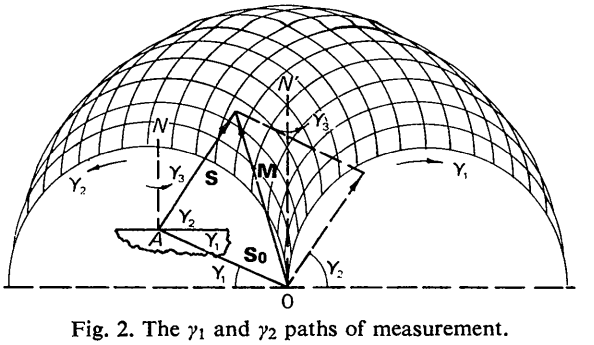

Fig. 2. The γ_1 and γ_2 paths of measurement.

After substituting equation (2) into equation (3), it is noted that γ_r and γ_p are dependent variables when combined at the measuring point, **M**. Also, since the receiving Soller slit sees radiation from more than one point in the primary Soller slit, the combined effect of the Soller slits at **M** is

$$L(\gamma_s'-\gamma_s)=\int L_p(\gamma_s'-\gamma_s-\bar{\gamma}_s)\, L_r(\bar{\gamma}_s)\, d\bar{\gamma}_s \qquad (4)$$

where γ_s is the rotation about a horizontal line lying on the specimen surface. The relation between the angles γ_3 and γ_s is

$$\gamma_3=\text{arc sin}\,(\tan\gamma_s/\sin|(\gamma_2'-\gamma_1')/2|)\,. \qquad (5)$$

A change of $L(\gamma_s)$ must be made with the variable change to give $h(\gamma_3)$. Along with this change in variable, the absorption path length becomes independent of γ_3. In addition, if the divergence of γ_1 is small as in the use of a monochromator, the absorption path length may be assumed to be only a function of γ_2 for a fixed γ_1 and may be combined with $S(\gamma_2/a_r)$ to give

$$g(\gamma_2'-\gamma_2)=\int S\left(\frac{\gamma_2'-\gamma_2-\bar{\gamma}_2}{a_r}\right) A(\gamma_1',\bar{\gamma}_2)\, d\bar{\gamma}_2 \qquad (6)$$

where

$$A(\gamma_1',\bar{\gamma}_2)=\int_{\gamma_2'-b}^{\gamma_2'+c}\exp\{-\mu a(\gamma_1',\gamma_2)\}d\gamma_2\,. \qquad (7)$$

The absorption path length for one path is given by

$$a(\gamma_1',\gamma_2)=R\,\frac{\gamma_2'-\gamma_2}{\sin(\gamma_1'+\gamma_2')}\left[1+\frac{\sin\gamma_1'}{\sin\gamma_2'}\right] \qquad (7a)$$

where R is the specimen to observation distance. The limits of the integral in equation (7) are given by the possible limits of γ_2 due to the spread of the beam on the sample.

Incorporating these changes in equations (2) and (3) yields

$$P(\gamma_1',\gamma_2',\gamma_3')=\iiint I(\gamma_1,\gamma_2,\gamma_3)f(\gamma_1'-\gamma_1) g(\gamma_2'-\gamma_2)\,h(\gamma_3'-\gamma_3)\,d\gamma_1 d\gamma_2 d\gamma_3\,. \qquad (8)$$

The function $f(\gamma_1)$ must be experimentally determined since it is dependent on the intensity variation of the source. In addition, the primary Soller slit function $L_p(\gamma_p)$ is dependent on the source variation and is given by

$$L_p(\gamma_p)=(1-|\gamma_p/a_p|)\,T(\gamma_p) \qquad (9)$$

where a_p is twice the ratio of the separation to the length of the Soller slits, and $T(\gamma_p)$ is the source variation in γ_p. After determining $T(\gamma_p)$, the function $L(\gamma_s)$ may be calculated from equations (4) and (9) where $L_r(\gamma_r)$ is of the same form as $L_p(\gamma_p)$ with $T(\gamma_r)$ a constant since the response of the detector does not have an appreciable variation over the slits. The third function, $g(\gamma_2)$, may be calculated from equations (6), (7) and (7*a*) for each particular set of experimental variables.

As shown in equation (8), measuring at fixed values of the variables yields a weighted integrated intensity. To eliminate the instrumental functions, a series of measurements along each coordinate must be obtained. For example, measurements along γ_1 at fixed γ_2 and γ_3 gives

$$P(\bar{\gamma}_1,\gamma_2',\gamma_3')=\int P_{\text{proj}}(\gamma_1,\gamma_2',\gamma_3')f(\bar{\gamma}_1-\gamma_1)\,d\gamma_1 \qquad (10)$$

where $P_{\text{proj}}(\gamma_1,\gamma_2',\gamma_3')$ is a weighted projection of $I(\gamma_1,\gamma_2,\gamma_3)$. Equation (10) may be solved for $P_{\text{proj}}(\gamma_1,\gamma_2',\gamma_3')$ for various values of γ_2' and γ_3' resulting in a function independent of $f(\gamma_1)$. By following a similar procedure $g(\gamma_2)$ may be eliminated and finally $h(\gamma_3)$ may be eliminated to give $I(\gamma_1,\gamma_2,\gamma_3)$ independent of the instrument. The intensity determined at this point still contains the effect of the wavelength distribution which has been ignored in this study because of the difficulty in determining a function to describe this effect.

Instrument analysis

The measurements were made with Cu $K\beta$ radiation from a quartz curved-crystal monochromator to give a line source. A (10·1) plane of a quartz crystal with a bent radius of 57·3 mm was used in this study. The monochromator was set to focus on the specimen, and the width of the beam at the focal spot was 0·28 mm.

The 57·3 mm radius horizontal diffractometer employed pulse magnetic drives for a rotation of the specimen and rotation of the counter about a vertical axis. The third rotation of the specimen about its normal was accomplished by a single section of a universal goniometer. The detector was a Norelco proportional counter type 6232. The output of the counter was recorded with a scaler and printer, the magnetic pulse drives being driven by the pulse actuating the printer. Consequently, all power measurements were obtained by a fixed point count.

The functions which depend on the source distribution were determined by making measurements on the primary beam without a specimen. The function $f(\gamma_1)$, was determined by scanning the primary beam distribution with a divergence slit of 0·89° which was used throughout this study. From this measured distribution which is a convolution of the slit function and the source distribution, $f(\gamma_1)$ shown in Fig. 3 was calculated. The variation of the source intensity, $T(\gamma_p)$, across each Soller slit was measured with the use of a one-sided slit to give

$$P(\gamma_p)=\int_{-\infty}^{\gamma_p} L_p(\gamma_p)\,d\gamma_p \qquad (11)$$

shown in Fig. 4. The measured distribution, $P(\gamma_p)$, is shown in Fig. 4 along with the calculated distribution for $T(\gamma_p)$ assumed to be a constant. Since the measured distribution coincides with the calculated distribution the source variation, $T(\gamma_p)$, may be taken as a constant. Consequently, $L(\gamma_s)$ shown in Fig. 5 was calculated

from equations (5) and (9) with $a_p = 0{\cdot}00901\ r$, $a_r = 0{\cdot}00635\ r$, and $T(\gamma_p) = 1$. Since $h(\gamma_3)$ depends on the values of γ_2' and γ_1' in equation (5), it was calculated for each particular measurement. Also, the function $g(\gamma_2)$ which depends on the experimental variables must be calculated for that particular experiment.

Measurements were obtained with a freshly cleaved surface of a calcite single crystal whose orientation in the instrumental coordinates is given in Table 1.

Table 1. *Orientation of calcite in instrumental coordinates*

	Degrees		
Peak	γ_1	γ_2	γ_3
10·4	13·28	13·28	
21·10	22·20	50·14	18·00
22·6	5·00	70·08	−15·75

The instrumental functions $g(\gamma_2)$ and $h(\gamma_3)$ for the calcite (21·10) peak were calculated from equations (5), (6), (7), and (7*a*). Measurements for many combinations of the variables were made, and the measurements along each of γ_1, γ_2, and γ_3 through the maximum are shown in Figs. 6, 7, and 8. These measurements are representative of the shape of the curves for all other combinations of the variables. In addition, Figs. 6, 7, and 8 show the respective instrumental curves. The shape of the projected power distribution calculated from the solution of a one-dimensional convolution of the type given by equation (10) was calculated for each path of measurement. The calculated projected power distribution was symmetric and of the same general shape in all three cases. The width at half-height was approximately 0·005° in all three cases.

Measurements were also obtained from a freshly cleaved surface of a zinc single crystal. The instrumental function, $g(\gamma_2)$, was calculated from equations (7) and (7*a*), and the instrumental function $f(\gamma_1)$ was the same as used for calcite. The measured power curves, instru-

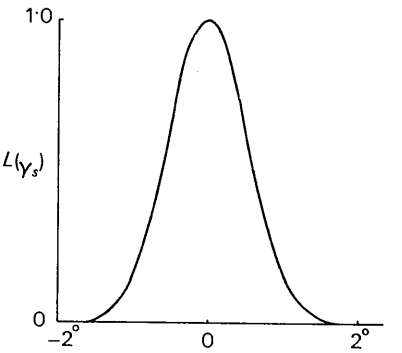

Fig. 5. Combined Soller slit function, $L(\gamma_s)$.

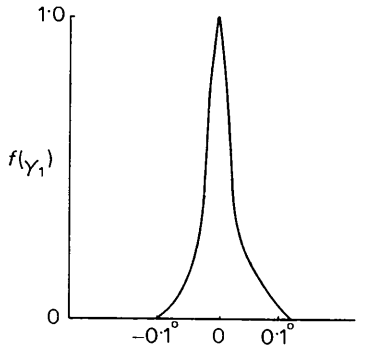

Fig. 3. Measured source function, $f(\gamma_1)$.

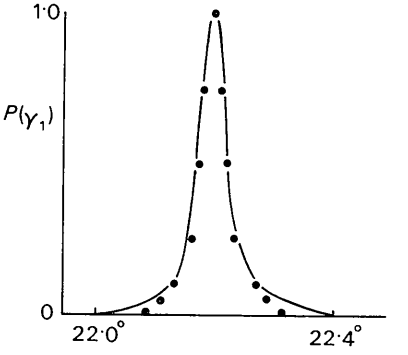

Fig. 6. Profile of calcite (21·10) along γ_1 for $\gamma_2 = 50{\cdot}14°$ and $\gamma_3 = 18{\cdot}00°$. The points correspond to $f(\gamma_1)$.

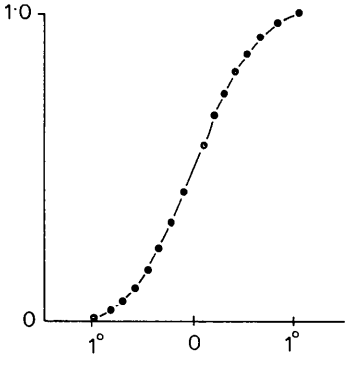

Fig. 4. Integral of the source function, $L_p(\gamma_p)$. The points are measured values and the line segments the calculated values for a constant source distribution.

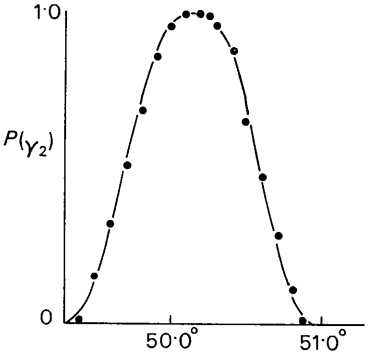

Fig. 7. Profile of calcite (21·10) along γ_2 for $\gamma_1 = 22{\cdot}20°$ and $\gamma_3 = 18{\cdot}00°$. The points correspond to $g(\gamma_2)$.

mental functions, and the resulting projected power curves along γ_1 and γ_2 through the maximum of the (00·4) peak are shown in Figs. 9 and 10.

Conclusions

The good agreement in Figs. 6, 7, and 8 of the measured power curves with the instrumental curves calculated for the calcite crystal verify the concept of the measuring functions. In particular, the functions $f(\gamma_1)$ and $h(\gamma_3)$ are in excellent agreement. However, the function $g(\gamma_2)$ does not agree as well as the other two functions with the measured distribution. The assumption that γ_1 is a constant in equation (6) accounts for a small part of the error, and probably the largest error is involved in the calculation of the limits of integration in equation (7). These limits are calculated from the width of the beam on the specimen, and the measurement of the beam width is open to error since one must choose a cut-off point.

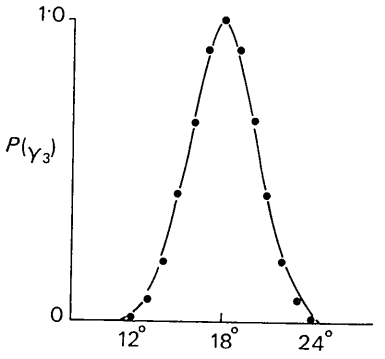

Fig. 8. Profile of calcite (21·10) along γ_3 for $\gamma_1 = 22{\cdot}20°$ and $\gamma_2 = 50{\cdot}14°$. The points correspond to $h(\gamma_3)$.

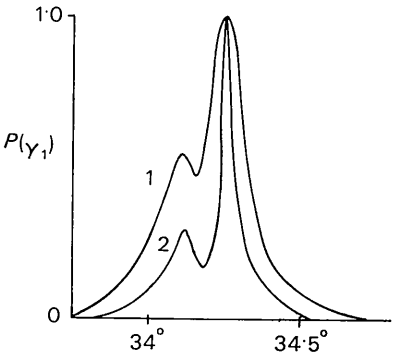

Fig. 9. Profile of zinc (00·4) along γ_1 for $\gamma_2 = 34{\cdot}25°$ and $\gamma_3 = 0°$. Curve 1 is the measured profile and curve 2 is the calculated projected intensity independent of $f(\gamma_1)$.

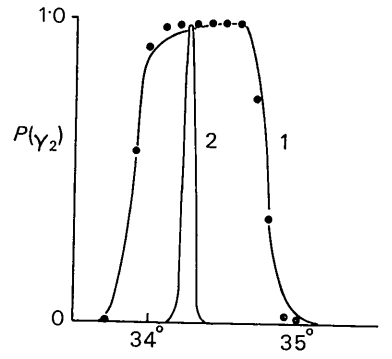

Fig. 10. Profile of zinc (00·4) along γ_2 for $\gamma_1 = 34{\cdot}25°$ and $\gamma_3 = 0°$. Curve 1 is the measured profile and curve 2 is the calculated projected intensity independent of $g(\gamma_2)$. The points correspond to $g(\gamma_2)$.

In the measurements shown in Figs. 9 and 10 of the zinc (00·4) peak, there are two points to consider. First, the measured curve as well as the calculated projected power curve along γ_2 indicate a single symmetric peak. Second, the curves for measurements along γ_1 in Fig. 9 indicate the presence of two peaks. A radial measurement, the normal Bragg–Brentano method, also indicated only a single peak but somewhat broadened on the low angle side. A series of radial measurements for small variations in the 2:1 coupling appreciably altered the asymmetry of the curve as the measurements along γ_1 would indicate. A projected measurement of both peaks would be possible only if both peaks lie within the measuring volume. Hence, for narrower slits than used in this study, it would be possible to measure only one peak. However, a slight misalignment could have an appreciable effect on the shape of the curve. Consequently, the recorded one-dimensional power distribution may depend not only on the extent of the measuring volume but also on a slight misalignment of the instrument.

The large slit widths used in this study were chosen to illustrate the instrumental broadening and were not intended to be used for accurate line shape measurements, Therefore, the calculated projected power distributions along γ_2 and γ_3 were not accurate since we are concerned with small differences in broad curves. In using this approach to obtain three-dimensional line shapes, the slits chosen would necessarily be much narrower.

The more common single-crystal goniostats employing the Eulerian angles and pinhole collimators are more desirable for determining information concerning the specimen. However, a detailed three-dimensional instrumental analysis of the instrumental broadening is complicated by the difficulty in determining the source distribution. Also, an added problem is encountered since the 2θ measurements are affected by a variation in all the instrumental broadening effects. Furthermore, the rotation of the sample about its normal is also affected by the variation of more than one instrumental variable.

Although the particular instrumental coordinates chosen for this study are not the best set for most diffraction studies, they illustrate the concept of the three-dimensional measuring volume and the effects of a limited number of instrumental variables for each

path of measurement. Most line shape measurements would not require such a detailed study and expenditure in time, but the three-dimensional aspect of the measurement should be acknowledged in the interpretation of the results. A second path of measurement through the diffraction maxima may indicate if there are any problems encountered from broadening in the other directions.

The authors would like to acknowledge the support of this study by the National Science Foundation.

References

ALEXANDER, L. E. (1948). *J. Appl. Phys.* **19**, 1068.
ALEXANDER, L. E. (1950). *J. Appl. Phys.* **21**, 126.
ALEXANDER, L. E. (1954). *J. Appl. Phys.* **25**, 155.
ALEXANDER, L. E. & G. S. SMITH (1962). *Acta Cryst.* **15**, 983.
JONES, F. W. (1938). *Proc. Roy. Soc.* A, **166**, 618.
RAUTALA, P. & L. HYVÄRINEN (1955). *Ann. Acad. Sci. Fennicae*, Ser. A, I, 192.
SPENCER, R. C. (1931). *Phys. Rev.* **38**, 618.
SPENCER, R. C. (1939). *Phys. Rev.* **55**, 239.
SPENCER, R. C. (1949). *J. Appl. Phys.* **20**, 413.
STOKES, A. R. (1948). *Proc. Phys. Soc.* **61**, 382.

Acta Cryst. (1965). **18**, 686

Macroscopic Characteristics of Ribonuclease Crystals of Modifications I and II*

BY MURRAY VERNON KING†

Polytechnic Institute of Brooklyn, Brooklyn, N.Y. 11201, *U.S.A.*

(*Received* 7 *March* 1963 *and in revised form* 20 *July* 1964)

The morphology and mechanical properties of crystals of modifications I and II of bovine pancreatic ribonuclease are described and discussed in the light of proposed molecular packings.

It is of interest to correlate such macroscopic characteristics of protein crystals as their morphology, etch symmetry, and cleavage or fracture with postulated models of the molecular packing within the crystals. Some electron-microscope studies (*e.g.* Labaw & Wyckoff, 1957; Labaw, 1959) of large molecules such as the viruses have directly revealed the packing of the molecules on various crystal faces. However, an electron-microscope study of a smaller protein, bovine pancreatic ribonuclease (Dawson & Watson, 1959) showed some detail in the form of striation of the faces, but did not give complete resolution of neighboring molecules. In such a case, we may find it especially useful to infer the molecular packing from X-ray diffraction data, and correlate this packing model with the observed morphology and other macroscopic characteristics.

The present study is concerned with the morphology, cleavage, and fracture of bovine pancreatic ribonuclease crystals of modifications I and II, which have been previously reported (Fankuchen, 1941; Fankuchen, 1945; Carlisle & Scouloudi, 1951; King, Magdoff, Adelman & Harker, 1956; the latter reference is hereinafter denoted as KMAH).

Harker (1957) has proposed molecular packing models for these modifications on the basis of symmetry and steric packing considerations, and has kindly supplied by private communication the values of the molecular parameters on which his packing diagrams are based. These values are corroborated by the arrangement of peaks in the low-resolution (10 Å) three-dimensional Patterson functions of these modifications. For form I, the molecular centroids are in positions 4(*a*) of space group $P2_12_12_1$ with $x=0{\cdot}00$, $y=0{\cdot}00$, $z=0{\cdot}25$, as corroborated by Patterson peaks at $0\frac{1}{2}0$, $\frac{1}{2}0\frac{1}{2}$, and $\frac{1}{2}\frac{1}{2}\frac{1}{2}$. For form II, the molecular centroids predicted by packing considerations are in positions 2(*a*) of space group $P2_1$, with $x=0{\cdot}17$, $y=0{\cdot}50$, $z=0{\cdot}74$.

For convenience, the following abbreviations will be used: RNase = bovine pancreatic ribonuclease; MPD = 2-methyl-2,4-pentanediol.

Experimental

The bulk of the crystals studied here were prepared and preserved by standardized methods described elsewhere (King, 1964*a*).

Observations of morphology and cleavage or fracture were made upon crystals immersed in a portion of their preserving solution held in a microscope slide having a flat-bottomed well; the specimens were kept covered with cover glasses at all times to prevent evaporation, except when the crystals were being manipulated mechanically. Interfacial angles were measured under a polarizing microscope having a rotating stage.

* Contribution from the Protein Structure Project, Polytechnic Institute of Brooklyn.

† Present address: Orthopedic Research Laboratories, Massachusetts General Hospital, Boston 14, Massachusetts, U.S.A.